A Microwave Spot Probe Method for Scanning Aircraft Radomes

Ryan FREEMAN, Brian PETRIE, John W. SCHULTZ

Compass Technology Group; Alpharetta GA, USA
e-mail: ryan.freeman@compasstech.com, brian.petrie@compasstech.com, john.schultz@compasstech.com

Nihad ALFAYSALE

Material and Manufacturing Directorate / ManTech division, Air Force Research Laboratory
e-mail: nihad.alfaysale.2@us.af.mil

Abstract
We present an NDT method for detecting mechanical defects in radomes. The technique is based on analysis of microwave spectra measurements captured from handheld spot probes. The measurements are processed using microwave transmission line theory, and empirical lineshape fitting, with the results of the processing providing the likelihood of the presence of defects. Here, we show measurements and modeling to detect delaminations between the core and shell of an A-sandwich radome, as well as water trapped in the radome core. We also show proof of principle results indicating that a similar NDT defect detection method can be developed for use from 20 to 40 GHz, for both X-band dielectric radomes, as well as higher frequency millimeter wave radomes.

Keywords: radome, microwave, spot probe

1. Introduction

Non-destructive testing (NDT) of radar-active components for aerospace applications generally involves processes to check for both mechanical integrity and electromagnetic (EM) performance. As the components are used in the field, natural degradation makes it necessary to test the quality of the components throughout their lifetimes and inform decisions regarding repairs and maintenance. These NDT processes often involve various types of equipment and rely on expert interpretation of the technical testing results [1]. In this paper, we present a microwave defect detection system for NDT testing of dielectric radomes. We show a working implementation of the defect detection designed for use from 2-18 GHz with the Compass Technology Group SP218 microwave spot probe shown in Figure 1a (and the Copper Mountain Technologies RP180 vector network analyzer, VNA). We also show proof of principle experiments and modeling to show how a similar system can be developed for use from 20-40 GHz (Figure 1b).

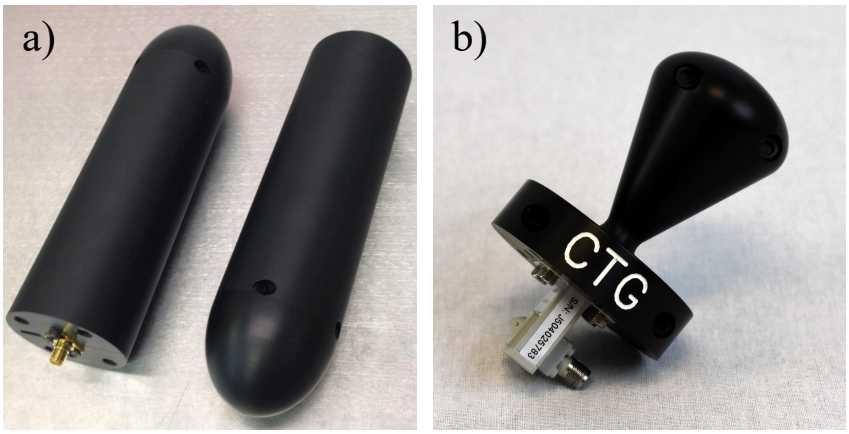

Figure 1: Images of microwave spot probes used to measure radomes for defect detection: a) CTG's SP218 spot probe and b) CTG's SP2040 spot probe.

The measurement system launches EM energy at a roughly 2 inch spot on the surface of the radome [2], and captures reflected EM spectra as a function of frequency. The reflection spectra are processed to determine acceptable electromagnetic performance and trends in the spectra can indicate the likelihood of mechanical defects. The presented system provides a convenient solution to test mechanical and electromagnetic integrity of radomes in situ, with spatial resolution on the order of an inch or so. This represents a general NDT approach that can be applied to various dielectric, radar-active components using measurement devices that capture electromagnetic spectra.

Radomes are dielectric shells surrounding radar elements that shield the radar elements from hazardous environments and provide EM transparency in frequency ranges. Radomes are generally composed of low-loss dielectric materials, such as plastics or fiberglass composites. In aerospace applications, they protect against aerodynamic loads, thermal cycling, and weather erosion. The working principle of the radome can be understood by first discussing the simple case of a plane wave incident on a lossless dielectric slab. In this case, there are resonances in the reflectivity at frequencies where reflected waves from the inner and outer surface of the radome are out of phase. This interference leads to minimized reflection and maximized transmission. The radome resonance frequencies can be written as:

$$f_{res} = \frac{nc}{2d\sqrt{\varepsilon - \sin^2\theta}} \qquad (1)$$

where d is the thickness, ε is the permittivity, c is the speed of light in vacuum, θ is the incidence angle, and $n=1,2,3\ldots$ is the order of the resonance [3]. The parameters of the radome are chosen so that one of the resonances aligns with the operating frequency of the radar.

The above expression applies to a monolithic slab however, multilayer radome configurations are also used. In these cases Equation (1) is no longer valid, but the overall working principle is the same. Common radome configurations are shown in figure 2, and include the "A-sandwich" where two dielectric slabs are separated by a low-dielectric spacer, the "B-sandwich" where a dielectric slab is interfaced with two low-dielectric layers, and the "C-sandwich" where three dielectric slabs are separated by two low-dielectric spacers. The low-dielectric spacer material can be foam or honeycomb and sets the spacing between the dielectric layers controlling the resonance frequency while providing mechanical stiffness.

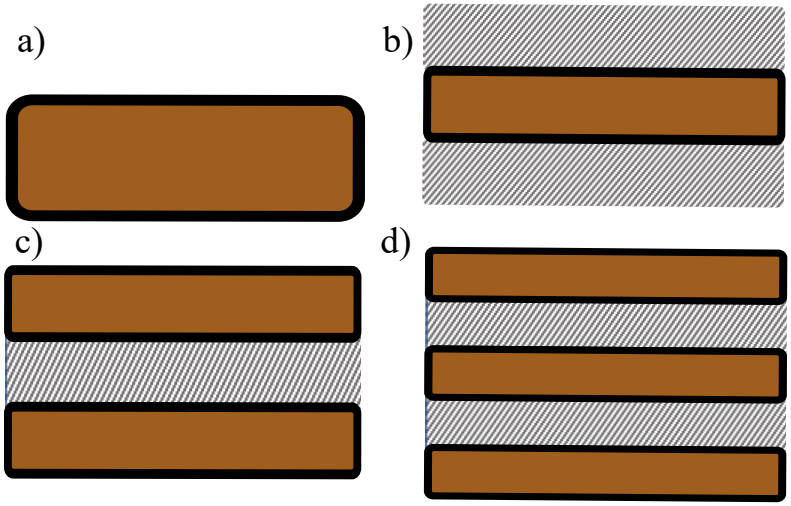

Figure 2: Schematics of Common Radome Configurations:
a) Monolithic b) B-sandwich c) A-sandwich d) C-sandwich

There are several common defects that affect both the mechanical stability of radomes, as well as their electromagnetic properties. Weather can erode the outer radome surfaces, making the radome thinner. Radomes with foam or honeycomb core can trap water within the cavities of the core. Radomes made of plies of fiberglass composites can delaminate due to mechanical stresses. When these defects become extreme the radome can fail mechanically, but even before critical failure defects begin to affect electromagnetic performance. Radomes are resonant structures, and small changes in the resonator can have large effects on the resonance.

2. Analyzing Reflection Spectra

The physical properties and electromagnetic performance of a radome are intrinsically linked. For this reason, the reflection and transmission spectra of a radome can hold valuable information about the physical make-up of the radome. The following shows two approaches to correlate the measured reflection spectra with the likelihood of different radome defects: i) physics-based EM modeling and ii) empirical analysis of the spectral lineshape. For the first approach, the measured spectra is compared to modeled spectra and parameters representing the radome, such as the thicknesses of the different layers or their dielectric properties, are adjusted to optimize the model/measurement agreement. Extracting physical parameters from a measurement is referred to as an 'inversion' algorithm, which extracts these parameters by fitting to a realistic model of the system. For example, we can measure a three-layer radome and invert the thicknesses of each layer.

Here, we show how the likelihood of radome defects can be predicted based inversions using one dimensional microwave transmission line theory. In this model, a sample is defined by the thickness, d_i, electric permittivity, ε_i, and magnetic permeability, μ_i, of each layer. This model accounts for the fields reflected at and transmitted through each interface in the sample. We evaluate the interaction of the radiation from the spot probe with the sample, in this case a radome, in the formalism of a two-port network [4]:

$$\begin{bmatrix} b_1 \\ b_2 \end{bmatrix} = \begin{bmatrix} S_{11} & S_{12} \\ S_{21} & S_{22} \end{bmatrix} \begin{bmatrix} a_1 \\ a_2 \end{bmatrix} \tag{2}$$

where a_i represent the input voltages, b_i represent the output voltages, and S_{ij} represent the scattering coefficients. In our application, the spot probe measures S_{11}. For a single slab, the S matrix can be written simply in terms of the material thickness, permittivity and permeability. Radomes are generally nonmagnetic, so we set $\mu_i = 1$. For multiple layers, the S matrix formalism becomes messy, so the scattering equation above is conveniently reformulated into:

$$\begin{bmatrix} b_1 \\ a_1 \end{bmatrix} = \begin{bmatrix} R_{11} & R_{12} \\ R_{21} & R_{22} \end{bmatrix} \begin{bmatrix} a_2 \\ b_2 \end{bmatrix} \tag{3}$$

This formulation has the useful property that each layer can be represented by a separate scattering matrix R_i, which are then multiplied together:

$$\begin{bmatrix} b_1 \\ a_1 \end{bmatrix} = \prod [R_i] \begin{bmatrix} a_2 \\ b_2 \end{bmatrix} = [R_{total}] \begin{bmatrix} a_2 \\ b_2 \end{bmatrix} \tag{4}$$

We use this expression to model the radome, with each layer represented by a separate R matrix as a function of the layer thickness, d_i, and permittivity, ε_i. The total R matrix is then transformed back into the S-matrix, and the frequency-dependent S_{11} is calculated. This gives us the ability of inverting the properties of the radome from the measured S_{11} spectra, by adjusting the thicknesses or permittivities in the model to minimize the difference between

model and measurement. The inverted material parameters then provide indications of radome health and defect likelihood.

The second approach to analyzing reflection spectra is through empirical fitting. We have identified two expressions that accurately describe the radome's reflected amplitude and phase spectra respectively. These expressions are not based on derivations, rather they are an empirical description of the spectra captured from radomes. The reflection amplitude spectra, featuring the prominent radome null, can be fitted with a Lorentzian null, superimposed on top of a linear background:

$$S_{11,amp}(f) = (a_1 + b * f) * \left(\left(\frac{a_2}{\pi}\right) * \frac{{}^{w}/_{2}}{(f - f_0)^2 + \left({}^{w}/_{2}\right)^2} + 1 \right) \quad (5)$$

The reflection phase spectra, exhibits a phase shift at the radome's resonant frequency, and can be fitted to the following:

$$S_{11,phase}(f) = a_1 + b * f + a_2 * \tanh\left({}^{(f - f0)}/_{w}\right) \quad (6)$$

where in both expressions f denotes frequency, a_1 is a frequency-independent offset, b is the overall slope, f_0 is the frequency of the radome null, a_2 is the amplitude of the null, and w is the linewidth of the null. In this approach the amplitude and phase spectra are measured and then fit to the above expressions. The resulting five fit parameters from each spectra can then be analyzed to show whether the radome is healthy or defective.

We used both these two approaches to analyze measurements of reflection spectra from radomes. By studying what these fits and inversions return for both healthy and defective radomes, we developed a method to predict radome health. However, there are limitations to these approaches that complicate the method. For instance, the inversion algorithm must be primed with an initial guess of the fit parameters, and the quality of the fit can depend on this guess. Further, the inversion is based on a specific model, which makes assumptions about the radome structure. For example, if a dielectric slab is measured and thickness inverted, the model must assume a certain dielectric permittivity. If this permittivity is off, then the inverted thickness will be wrong. Finally, it can be difficult to fit or invert multiple parameters due to cross-correlations between the fitting parameters. As the number of fit parameters is increased the number of equivalent solutions also increases, making it harder to find the true solution.

In the context of testing potentially defective radomes, we are faced with tricky 'edge cases' that suffer from these complications. For example, an inversion based on a pristine model may not correctly describe a defective radome. Additionally, sample to sample variations can make it difficult to arrive at the same solution branch for each measurement. Our general strategy for dealing with these uncertainties is to carefully study the solution space of various inversion models and identify trends in each associated with common defects. By understanding how defects affect the solution space of the inversions, even 'wrong' solutions can give valuable information about the quality of the radome, and the likelihood of different defects.

3. Identifying Delamination

To understand the solution space of the lineshape fits and EM inversions and ultimately generate a defect detection method, we performed a series of experiments and simulations on healthy and defective radomes. As an example, we present studies of A-sandwich radomes designed with an X-band resonance ($f_0 \approx 9.7$ GHz), and with delaminations of increasing thickness between the shell and core. The shell material of the experimental radome is a 20-mil thick

autoclave-cured fiberglass composite, and the core material is 250 mil thick 'DuPont Nomex Honeycomb'. Reflection spectra of each individual component were measured with a handheld probe. Using microwave transmission line theory and the known physical thicknesses, we inverted the layer permittivities: $\varepsilon_{fiberglass} = 4.75 - 0.07i$ and $\varepsilon_{honeycomb} = 1.11 - 0.005i$.

We then assembled the radomes, adhering the layers together with a thinned solution of cement. We fabricated two pristine radomes and five delaminated radomes ($d_{delam} = 10, 20, 30, 40, 50$ mils). The delaminations were built into the radomes by inserting window spacers of 10 mil fiberglass between the outer shell and core. The result is a radome with an air gap of known thickness between the shell and core. The reflection spectra of each radome was measured (Figure 3a) and fit to a model of a pristine radome, with the permittivities above. The three inverted thicknesses as a function of the delamination are shown in Figure 3c and d.

We averaged the inverted fiberglass thicknesses from each radome and fit the inverted core thickness as a linear function of the delamination window thickness. This linear fit, extrapolated to $d_{delam} = 0$, gives us the honeycomb core thickness for the EM model that best describes the pristine radomes that were fabricated. This analysis yields an outer fiberglass thickness of 18.9 mils, a honeycomb thickness of 267.5 mils, and an inner fiberglass thickness of 20.5 mils, close to the real thicknesses of 20, 250, and 20 mils. The discrepancy between experiment and fit results are likely due to the effects of the adhesive, which are not captured by the EM model.

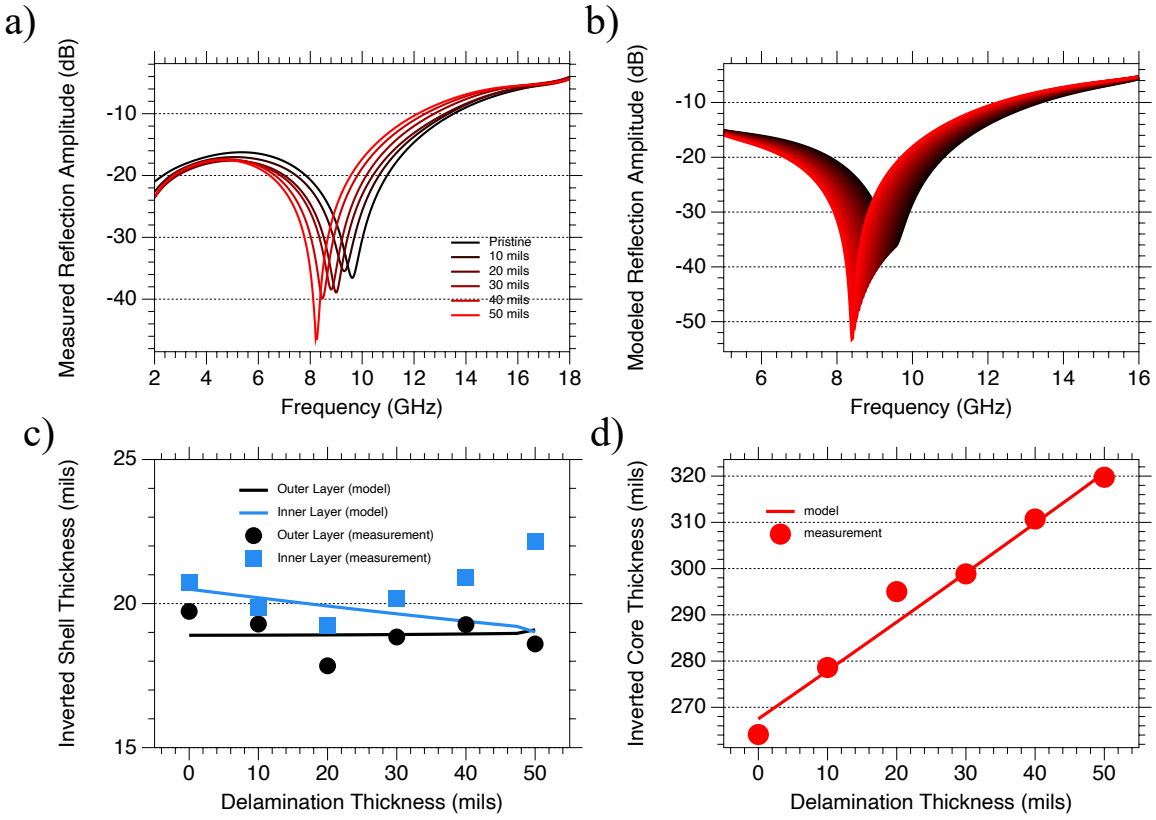

Figure 3: Measured and modelled reflection spectra from delaminated A-sandwich radomes: a) measured reflection for 6 different radomes with progressively larger delamination (black to red), b) modeled spectra as vs. delamination from 0 (black) to 50 mils (red), c) inverted shell thicknesses vs. the delamination, and d) inverted honeycomb core thickness vs. delamination.

Furthermore, this experiment is a clear example of how material parameter inversions can indicate the presence of defects. As the severity of a delamination is increased, a 3-layer thickness inversion returns larger honeycomb core thickness and total thickness, while returning shell thicknesses close to the pristine value. This makes sense as the honeycomb permittivity is close to that of air, $\varepsilon_{honeycomb} = 1.11 \approx \varepsilon_{air} = 1$. So the inversion 'chooses' a larger honeycomb layer thickness instead of a larger fiberglass layer thickness to account for the extra radome thickness introduced by the delamination.

We can gain additional confidence in the inversion trends by analyzing modeled spectra of delaminated radomes, using a 1D microwave model with the constituent permittivities and the pristine thicknesses extracted from the experiment detailed above. The delamination is modeled as a layer of air, separating the shell and core. The spectra generated by this model can be inverted by the same 3-layer thickness inversion to identify trends in the inverted parameters as the severity of the delamination is increased. Figure 3a and b compares the measured and modeled spectra of the delaminated radomes, showing agreement. The inversion trends of the modeled delaminated radomes are also similar to the trends identified in the experiment.

In addition to material inversions, the lineshape of the measured and modeled reflection amplitude and phase can also be fit using Equations 5 and 6 to identify delamination trends. Figure 4 compares the amplitude spectral lineshape of inner and outer interface delaminations, showing a clear difference between the lineshape of the inner and outer delamination. Most lineshape parameters show identical trends, but the linewidth of the radome null increases for outer delaminations and decreases for inner delaminations. This subtle difference between the spectra of the inner and outer delaminations is not identified by the 3-layer thickness inversions

We tested lineshape fit equations with fewer, and greater than the 5 fit parameters that were eventually chosen. More fit parameters allow for a more exact fit to the measured spectra but spread the effect of the defect amongst the additional parameters, making identification more difficult. Oppositely, fewer fit parameters makes the spectral lineshape fit worse, and the fit parameters jump abruptly between degenerate solutions or local minima as the severity of the delamination increases. Equations 5 and 6 were found to optimally model the radome's spectra and predict the presence of defects.

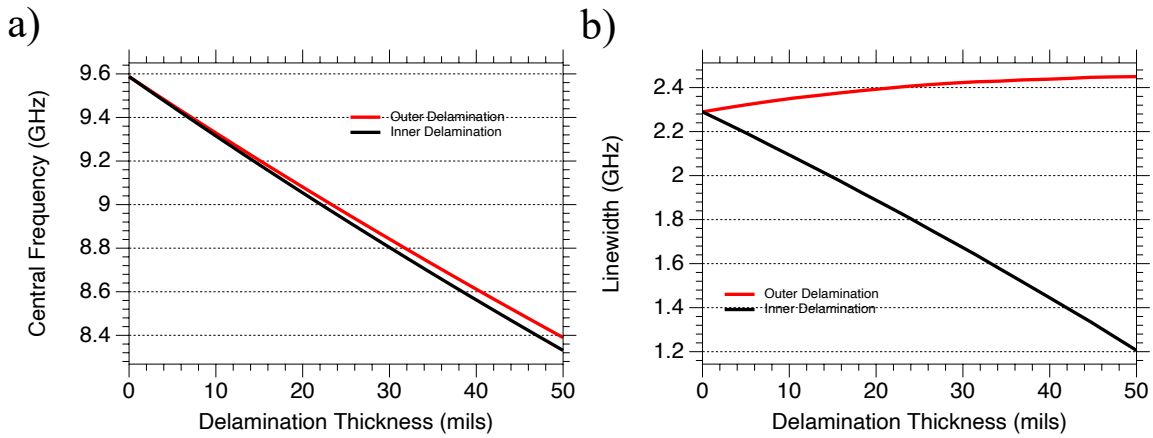

Figure 4: Spectral lineshape fit parameters: a) central frequency of radome spectra vs. delamination thickness and b) radome spectra linewidth vs. delamination thickness.

4. Additional Inversion Models & Defects

While the 3-layer thickness inversion is intuitive for radome analysis, there is no reason why other inversion models cannot also be used. The only requirements for successful parameter inversions are that the inversion models capture the relevant physics and the fit parameters exhibit relatively low cross-correlations. Besides the 1D microwave model implemented here, other model techniques, such as finite element, could be used. Furthermore, different combinations of fit parameters could be identified as long as they exhibit reasonably low cross-correlations and give accurate fits of the measurement.

Even with judiciously chosen initial guesses, sample to sample variations can make inversion models susceptible to physically inaccurate but mathematically acceptable solutions. The likelihood of an inversion getting trapped in bad solutions increases as defects are added into the mix, introducing discrepancy between the model and the physical specimen. A strategy for diminishing the effects of bad solutions is to use multiple inversions.

We studied different inversions based on the 1D microwave transmission line model to find robust inversions for radome analysis and studied the cross-correlations between the chosen inversion parameters. Inversions whose fit parameters exhibit low cross-correlations independently solve for each parameter and robustly find solutions. Alternately, models with excessive cross-correlations struggle to solve for each parameter independently and solutions will be unreliable. Cross-correlations can be calculated easily, whenever an inversion with multiple fit parameters is performed. The cross-correlation between two inversion parameters *a* and *b*, is a number between -1 and 1, and can be written as:

$$C_{ab} = \frac{\Omega_{ab}}{\sqrt{\Omega_{aa}\Omega_{bb}}} \tag{7}$$

where Ω is the covariance matrix of the inversion, which characterizes the fit quality and sensitivity to the chosen inversion parameters:

$$\Omega = \left({}^{\sigma}/_{(n-p)}\right)(X^T X)^{-1} \tag{8}$$

where σ is the fit residual, n is the number of measurement points, p is the number of inversion parameters, and $(X^T X)^{-1}$ is the inverse of the sensitivity matrix. The sensitivity matrix describes how sensitive the inversion model is to changes in the inverted parameters:

$$(X^T X)^{-1} = \sum_n \begin{bmatrix} \left({}^{\partial f}/_{\partial x_1}\right)^2 & \cdots & \left({}^{\partial f}/_{\partial x_1}{}^{\partial f}/_{\partial x_m}\right) \\ \vdots & \ddots & \vdots \\ \left({}^{\partial f}/_{\partial x_m}{}^{\partial f}/_{\partial x_1}\right) & \cdots & \left({}^{\partial f}/_{\partial x_m}\right)^2 \end{bmatrix} \tag{9}$$

where n is the number of measurement points, f is the function being fit, x_i are the fit parameters, and m is the total number of fit parameters. Using this cross-correlation analysis, we identified inversions that exhibited low cross-correlations and worked well for radome analysis. In practice, cross-correlations of less than 0.9 generally indicated effective inversions.

We studied several types of defects common to A-sandwich radomes and tried different inversion models to find trends for those defects. For brevity, we discuss only one more defect that is common to A-sandwich radomes: trapped water. While it is difficult for water to get into the core of a radome, once it is there the fiberglass makes it difficult for the water to leave. To experimentally study the effects of water content in the radome, we drilled 8 mil diameter holes into a 3” x 3” square region at the middle of a radome, and injected water into the honeycomb cells via a hypodermic needle, as shown in Figure 5. The EM model used to simulate the water-

logged radome was similar to the microwave models described above, with the addition of a thin water layer at either interface of the honeycomb and fiberglass. We model the frequency dependent permittivity of water using the Debye model [4,5]: $\varepsilon(f) = \varepsilon_\infty + \frac{\varepsilon_\infty - \varepsilon_{DC}}{1+i\cdot 2\pi f \cdot f_0}$, where $\varepsilon_\infty = 4.6$ is the permittivity in the high frequency limit, ε_{DC}=78.3 is the permittivity in the low frequency limit, and $f_0 = 124$ GHz is the characteristic relaxation frequency of water.

The following three inversions proved effective for detecting the presence of water:

1) Fitting the thicknesses of each of the three radome layers: the presence of water was associated with an increase in the inverted outer fiberglass thickness and a decrease in the honeycomb core and total radome thickness.
2) Fixing the thicknesses of the fiberglass layers to be equal to one another and fitting for the fiberglass and honeycomb thickness. The presence of water is again indicated by an increase in the fiberglass thickness and a decrease in the honeycomb and total radome thicknesses.
3) Assuming the water layer to be at the inner honeycomb/fiberglass interface and fitting for the thicknesses of the water and core layers. The presence of water is associated with a water film thickness of more than 0.5 mils.

a) b)

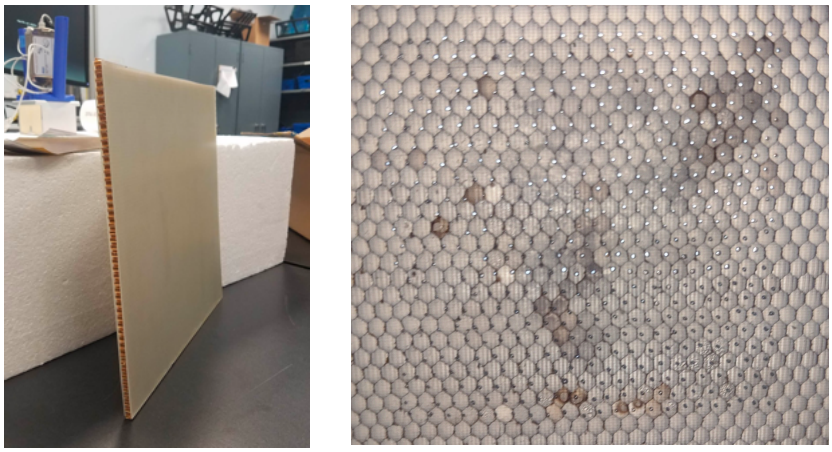

Figure 5: a) Image of experimental A-sandwich radome, b) close-up of water-logged radome, with water injected into cells via holes drilled into fiberglass shell.

The identification of trends in the inversions and lineshape fits associated with specific defects such as delamination and water allowed us to create a method to predict the likelihood of various defects based on reflection spectra measurements:

1. Measure S11 spectra with microwave spot probe from 2 to 18 GHz.
2. Compare measured spectra to the expected pristine radome spectra. If the difference between the measured and pristine spectra is above a certain threshold, the radome quality is questionable and further defect detection begins.
3. Inversions and spectral lineshape fits are performed. For each inversion, the inverted parameters are compared to a pristine radome. If the inverted parameters correlate with any specific defect, then a flag for that defect is recorded.
4. The defect reported is the one that has the highest percentage of total flags reported. For example, if 20% of water flags are registered, but 70% of delamination flags are registered, then the measured point is determined to most likely be a delamination.

The results of this method are shown for two radomes in Figure 6. Figure 6a shows the percentage of water and delamination flags recorded from radome measurements as a function of the proximity of the probe to the 3" x 3" water-logged central square of an A-sandwich radome. Figure 6b shows the percentage of water and delamination flags recorded for a delaminated radome based on 16 measurements taken along the surface.

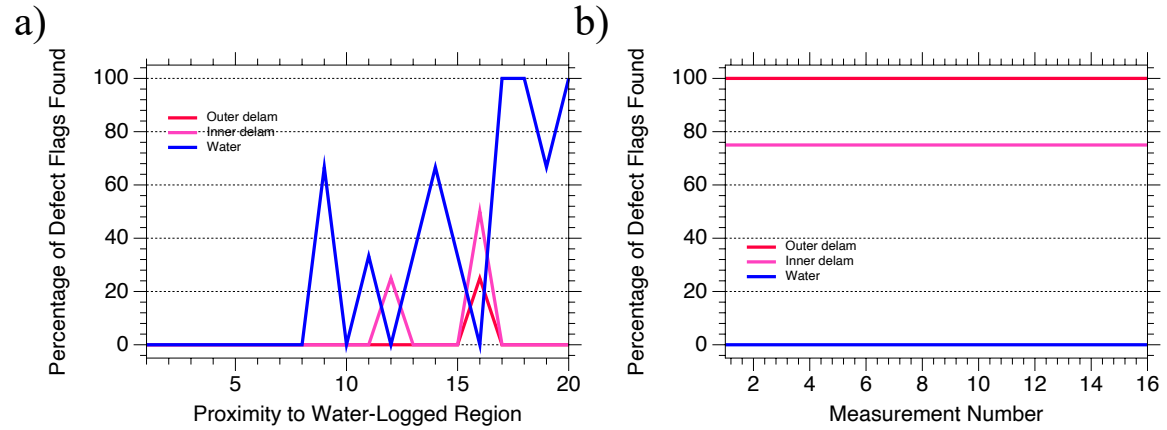

Figure 6: Results of defect detection algorithm: a) percentage of defect flags registered vs. proximity to the water-logged center of the radome and b) percentage of defect flags vs. measurement number, for 16 random points along surface of 10 mil delaminated radome.

5. Defect Detection from 20-40 GHz

The above discussion is based on modelling and measurement from 2 to 18 GHz. We recently developed a spot probe optimized for measurements from 20 to 40 GHz, called the SP2040. While this frequency band is critical for new '5G' technologies, radomes designed for lower frequencies, such as the X-band radome discussed in this paper will also have higher frequency radome nulls. In Figure 7, we show an experiment in which the X-band radome discussed throughout this paper is capped with painter's tape and measured with the SP2040 probe. A measurement is taken every 25mm, and the thickness of tape is inverted from the spectra showing that the technique is sensitive to the tape thickness.

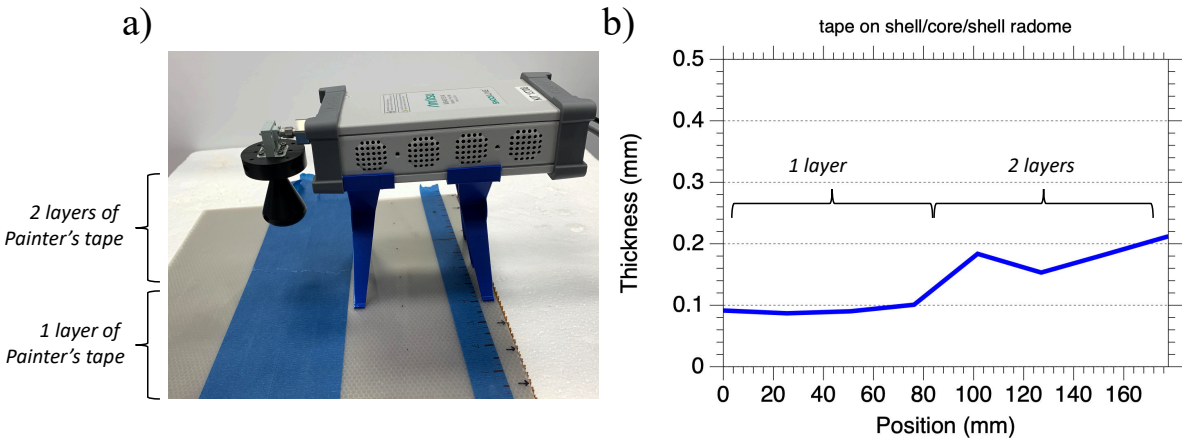

Figure 7: Proof of principle measurements from CTG's SP2040 probe: a) Image of SP2040 probe connected to an Anritsu MS46131A VNA and b) inverted thickness of painter's tape applied along the radome surface.

The full defect detection method outlined above can also be implemented for use with the millimeter wave spot probe. In fact the smaller wavelength can make defects even more obvious at these higher frequencies. As an example, figure 9 shows a modeled reflection spectra of an X-band radome, with different delamination thicknesses, from 5 to 50 GHz. The primary null at 9 GHz is shifted due to the presence of the delamination, but the higher order modes at 26 GHz and 45 GHz are affected even more strongly. This confirms that the SP2040 or other high frequency spot probes may be more sensitive to defects compared to lower frequencies.

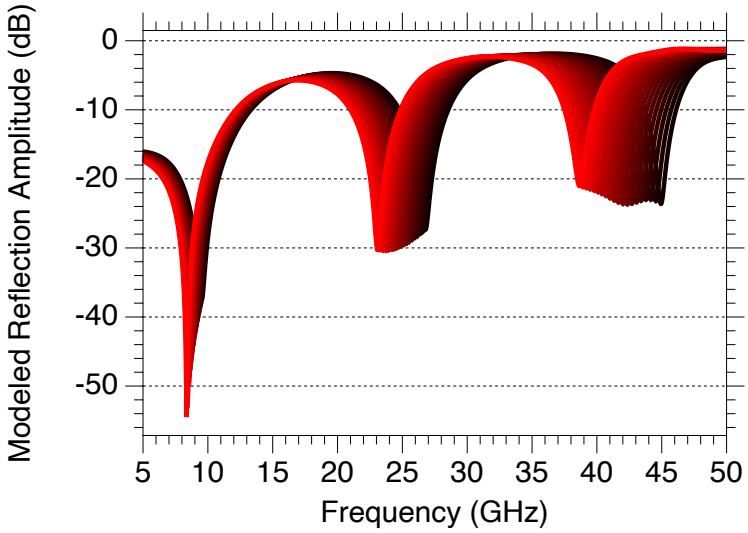

Figure 8: Modeled radome reflection spectra, as delamination thickness is increased from 0 (black) to 50 mils (red), plotted from 5 to 50 GHz.

6. Conclusions

We presented an NDT method for detecting mechanical defects in radomes. The technique is based on microwave spectra measurements, captured using microwave or millimeter wave spot probes. The measurements are processed using microwave transmission line theory and empirical lineshape fitting, with the results of the processing providing the likelihood of the presence of defects. This method of NDT is not limited to dielectric radomes, but can be applied to various types of dielectric components that exhibit distinctive microwave spectra in these frequency ranges.

References

1. C. Li *et al*., "A Review on Recent Progress of Portable Short-Range Noncontact Microwave Radar Systems," in *IEEE Transactions on Microwave Theory and Techniques*, vol. 65, no. 5, pp. 1692-1706, May 2017
2. J. Schultz, J. Maloney, K. Cummings, R. Schultz, J. Calzada, B. Foos, “A Comparison of Material Measurement Accuracy of RF Spot Probes to a Lens-Based Focused Beam System”, Proc. 2014 AMTA Symposium, 2014
3. R. Johnson, D. Burks, “Antenna Engineering Handbook”, McGraw-Hill, 1993
4. J. Schultz, “Focused Beam Methods: Measuring Microwave Materials in Free Space.” United States: CreateSpace Independent Publishing Platform, 2012
5. A. von Hippel, “Dielectric Materials and Applications”, Artech House, 1995